

Enforced symmetry breaking for valley polarization in two-dimensional hexagonal lattices

Yongqian Zhu,^{1,2} Jia-Tao Sun,^{3,*} Jinbo Pan,^{1,2,4} Jun Deng,¹ and Shixuan Du^{1,2,4,*}

¹*Beijing National Laboratory for Condensed Matter Physics, Institute of Physics, Chinese Academy of Sciences, Beijing 100190, China*

²*University of Chinese Academy of Sciences, Chinese Academy of Sciences, Beijing 100190, China*

³*School of Integrated Circuits and Electronics, MIT Key Laboratory for Low-Dimensional Quantum Structure and Devices, Beijing Institute of Technology, Beijing 100081, China*

⁴*Songshan Lake Materials Laboratory, Dongguan 523808, China*

The generation and manipulation of the valley polarization in solids are crucial for valleytronics, which is mainly limited to the analysis of inversion and time-reversal symmetries for two-dimensional (2D) hexagonal systems. Here, through group theory analysis, we propose general rules for the generation and manipulation of valley polarization in 2D hexagonal lattices. The generation of valley polarization requires breaking the specific enforced symmetry that is associated with different valleys or reverses the sign of Berry curvature. Further manipulation of valley polarization requires asymmetry operators connecting two states with opposite signs of Berry curvature. These rules for generating and manipulating valley polarization are extendable to generic points in momentum space. Combined with first-principles calculations, we realize the controllable valley polarization in three representative systems, i.e., monolayer FeCl₂, bilayer TcGeSe₃, and monolayer CrOBr. Our work provides symmetry rules for designing valleytronic materials that could facilitate the experimental detection and realistic applications.

I. INTRODUCTION

Valleytronics is a branch of electronics that utilizes valley degree of freedom (DOF) to process or store information [1,2], which lies in the generation and manipulation of valley polarization. The generation of valley polarization in 2D hexagonal lattices requires the breaking of both inversion and time-reversal symmetries, as revealed by studies of graphene [3-8], nonmagnetic transition metal dichalcogenides monolayer [9-19] (such as MoS₂, MoSe₂) and ferromagnetic monolayers (such as VSe₂ [20], LaBr₂ [21], VSSe [22] and LaBrI [23]). However, if an additional enforced symmetry is introduced, valley degeneracy is most likely constrained. For example, a stacked bilayer cannot exhibit valley polarization when it possess a combined symmetry of time-reversal and mirror symmetry with the normal vector along z axis [24]. Valley polarization requires a further breaking of the combined symmetry. Despite such examples, it lacks a systematic study on which additional symmetries must be broken to achieve valley polarization in 2D hexagonal materials, which hinders the development of general search and design strategies for identifying valley-polarized systems.

The manipulation of valley polarization requires reversibility, which can be achieved through various means such as switching the chirality of circularly polarized light [8,9,25-27], reversing the direction of external magnetic field [12], magnetic moment [20,21] or external electric field [28], or changing the stacking order [24,29]. Among them, the mechanism of the valley polarization reversal by switching the stacking order remains unclear. Researchers found that two states of monolayer VSe₂ connected by time-reversal operator with opposite magnetic moments exhibit opposite valley energy splitting and opposite Berry curvature distributions [20], suggesting their valley related properties are interconnected through the time-reversal operator. The connection between configurations and valley properties inspires us to consider whether an asymmetric transformation between two configurations of a bilayer structure will generate opposite valley polarizations. Moreover, previous studies on valley polarization were usually limited to the high symmetric momentum points without considering the generic momentum points, which significantly narrows down

the candidate materials for valleytronics.

In this work, based on systematic group theory analysis, we propose general symmetry rules for generating valley polarization and switching the valley DOF for 2D hexagonal systems. All the double Shubnikov space groups permitting valley polarization are identified. We reveal that the valley DOF associating two switchable states via the asymmetric connection operation can be switched. Interestingly, the connection operation also determines the coupling between valley, spin and layer DOFs, as well as the magnetoelectric coupling. Moreover, we generalize the location of valley to generic momentum points. Combined with first-principles calculations, we predict the reversible manipulation of valley polarization in three representative systems, i.e., monolayer FeCl₂, bilayer TcGeSe₃, and monolayer CrOBr.

II. GROUP THEORY ANALYSIS

We consider a 2D hexagonal system with spin-orbit coupling, whose valleys locate at the high symmetric K point in reciprocal space. We denote the symmetry operation as \hat{R}_S , where \hat{R}_S belongs to the double Shubnikov space group (DSSG) of the system and the subscript ‘‘S’’ of \hat{R}_S denotes ‘‘Shubnikov’’. The two states of valley DOF can be associated with positive and negative Berry curvatures [3,9,20]. In this sense, valley polarization requires not only a valley splitting but also a nonzero Berry curvature associated with valleys. As shown in the upper panel of Fig. 1, if existing a symmetry operator which connects two valleys at $+K$ and $-K$ points or reverses the sign of Berry curvature (Ω), valley degeneracy or zero net Berry curvature will be enforced (Table I and Sec. 1 of the Supplemental Material [30]). We refer to this symmetry as enforced symmetry. Valley polarization requires breaking the enforced symmetry to break valley degeneracy or induce nonzero net Berry curvature. For example, for the DSSG $P321$, a zero net Berry curvature will be enforced by the twofold rotational symmetry 2_{100} , which need to be broken to generate valley polarization. Hence, we obtain a symmetry rule for the generation of valley polarization, i.e., all the enforced symmetry operators connecting the two valleys or reversing the sign of Berry curvature must be broken. According to this rule, five DSSGs ($P3, P312', P3m'1, P\bar{6}, P\bar{6}m'2'$) permitting valley

polarization are identified and referred to as valley-polarized group (G_v). Meanwhile, the other 62 DSSGs of 2D hexagonal lattices belong to non-valley-polarized group (G_{nv} , see [Table S1](#) [30]).

Although valley polarization is prohibited in a system with a non-valley-polarized group G_{nv} , it can be induced by transforming the group G_{nv} to G_v via breaking enforced symmetries, including external magnetic field, electric field or bilayer stacking. We derive that five/nine non-valley-polarized groups allow the generation of valley polarization under an out-of-plane magnetic/electric field ([Sec. 2](#) of the Supplemental Material [30]). In the case of the bilayer stacking, we consider the homobilayer (B) in which the corresponding single layer (S) and $B = S + \hat{O}S$, where $\hat{O} = \{O|\mathbf{t}_o\}$ is a stacking operator with rotational part O and translational part \mathbf{t}_o [31]. We focus on the single-layer ferromagnet (FM) with out-of-plane magnetic moment, and the stacking bilayer with interlayer FM or antiferromagnetic (AFM) orderings. We consider a high symmetric stacking bilayer with the interlayer translation $\mathbf{t}_o = (\frac{1}{3}, \frac{2}{3})$ or $(\frac{2}{3}, \frac{1}{3})$, where the trivial out-of-plane translation is omitted. Its DSSG belongs to one of the groups $P3, P\bar{3}, P32'1, P3m'1, P\bar{3}m'1$ for the interlayer FM ordering or one of the groups $P3, P\bar{3}', P321, P3m'1, P\bar{3}'m'1$ for the interlayer AFM ordering, indicating that it can exhibit a spontaneous valley polarization or an induced valley polarization under an electric field. Hence, valley polarization can be induced in a magnetic monolayer either by stacking or by a combination of stacking and an electric field perpendicular to the interface. Besides, the generation of induced valley polarization in heterobilayers requires that the group of heterobilayer belongs to $P3$ or $P3m'1$ ([Sec. 2](#) of the Supplemental Material [30]).

Having identified the DSSGs allowing the generation of valley polarization, we then explore how to manipulate valley polarization (i.e., switching of valley DOF). We consider the switching between two valley-polarized states, state I and state II (lower panel of [Fig. 1](#)), of a system which are connected by an asymmetry operator, referred to as the connection operator (\hat{N}_S , the subscript ‘‘S’’ denotes ‘‘Shubnikov’’). In other words, state II is a transformation of state I under \hat{N}_S operation. Under the asymmetry

operation \widehat{N}_s , each physical quantity in Table I follows the same transformation rule as that under the symmetry operation \widehat{R}_s (Sec. 3 of the Supplemental Material [30]). Since the valley DOF is associated with Berry curvature, we obtain the rule for switching the valley DOF, i.e., a connection operation \widehat{N}_s is required to reverse the sign of Berry curvature. As the spin and net magnetization transform in the same way as Berry curvature, one can switch valley DOF via reversing spin and net magnetization through magnetic field. Particularly, when \widehat{N}_s can simultaneously reverse Berry curvature and layer (electric) polarization, valley DOF can also be switched by reversing layer (electric) polarization via electric field. Obviously, the connection operation \widehat{N}_s determines the manipulation methods of valley DOF, the coupling between valley, spin and layer DOFs, as well as the magnetoelectric coupling.

In fact, there are infinitely many \widehat{N}_s operations capable of switching valley DOF, such as the combination of an arbitrary rotation along z axis and time-reversal operation. However, only some of them are easy to realize in practical applications. For example, reversing the out-of-plane magnetic field or magnetic moment can switch valley DOF since $N_s = 1'$ reverses the sign of Berry curvature, where N_s is the rotational part of \widehat{N}_s . Meanwhile, flipping the out-of-plane electric field can switch valley DOF only when the corresponding \widehat{N}_s reverse the sign of Berry curvature (Sec. 3 of the Supplemental Material [30]). Additionally, for the switching of stacking orders, we consider two homobilayers with interlayer translation $\mathbf{t}_o = (\frac{1}{3}, \frac{2}{3})$ and $(\frac{2}{3}, \frac{1}{3})$, and assume that the direction of magnetic moment remains unchanged in the process of interlayer sliding. When they have interlayer FM ordering, the valley DOF cannot be switched by sliding because their connection operation \widehat{N}_s is forced to preserve the sign of out-of-plane magnetization and thus the sign of Berry curvature. Only when they have interlayer AFM ordering and spontaneous valley polarization, as well as $N_s \in \{2_{120}, m'_{001}\}G_3$, valley DOF can be switched by changing the stacking order. Besides, the valley DOF in heterobilayers can be switched by reversing the magnetization or changing the stacking order (Sec. 3 of the Supplemental Material [30]).

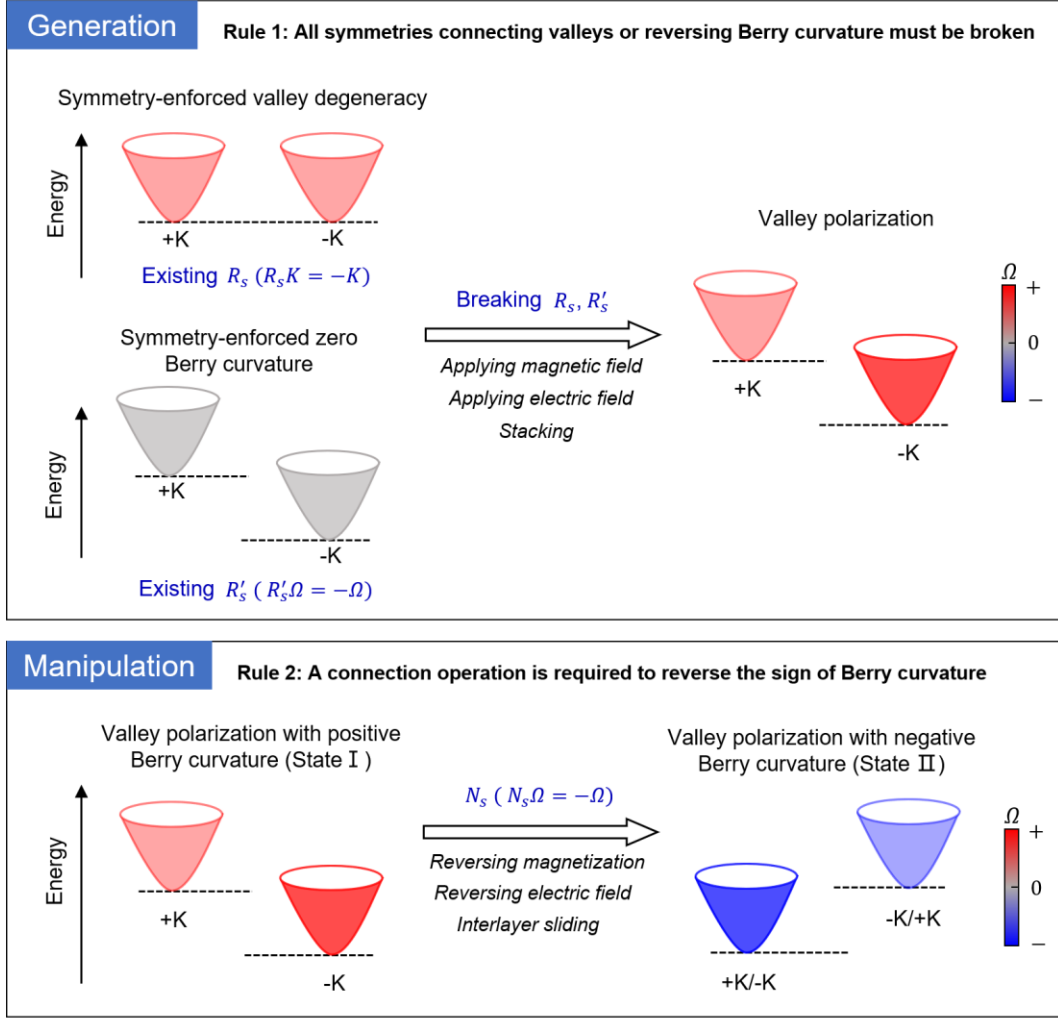


FIG. 1. The upper panel schematically illustrates the rule (Rule 1) for the generation of valley polarization. Left panels are two examples without valley polarization, while the right one is the valley polarization state. The valley polarization can be either spontaneous or induced by applying an external magnetic field, electric field or stacking. K is the high symmetry point in reciprocal space with the fractional coordinate $(1/3, 1/3)$. R_s is the rotational part (point group symmetry) of \hat{R}_s . The red, grey and blue colors denote the positive, zero and negative net Berry curvatures, respectively. The lower panel schematically illustrates the rule (Rule 2) for the manipulation of valley polarization. The two valley-polarized states with positive (state I) and negative (state II) Berry curvatures are connected by an asymmetry operator \hat{N}_s . N_s is the rotational part of \hat{N}_s . The manipulation methods include reversing the magnetization, reversing the electric field and interlayer sliding. K point maintains or reverses sign under \hat{N}_s operation.

TABLE I. Transformations under symmetry operations in 2D hexagonal lattices. The notations of operations follow the convention on the Bilbao Crystallographic Server [32]. The specific elements of the operation set $R_s G_3$ are listed in Table S2 [30], where $G_3 = \{1, 3_{001}^+, 3_{001}^-, d1, d3_{001}^+, d3_{001}^-\}$ denotes the double Shubnikov point group 3. s_z, Ω and P are the simplified denotations for z components of the spin vector, Berry curvature and electric polarization, respectively. L is the layer polarization [33]. “+”(“-”) denotes the preservation (reversal) of the sign of a physical quantity under an operation.

R_s, N_s	K	s_z, Ω	L, P	R_s, N_s	K	s_z, Ω	L, P
$1G_3$	+	+	+	$1'G_3$	-	-	+
$2_{001}G_3$	-	+	+	$2'_{001}G_3$	+	-	+
$2_{100}G_3$	+	-	-	$2'_{100}G_3$	-	+	-
$2_{120}G_3$	-	-	-	$2'_{120}G_3$	+	+	-
$\bar{1}G_3$	-	+	-	$\bar{1}'G_3$	+	-	-
$m_{001}G_3$	+	+	-	$m'_{001}G_3$	-	-	-
$m_{100}G_3$	-	-	+	$m'_{100}G_3$	+	+	+
$m_{120}G_3$	+	-	+	$m'_{120}G_3$	-	+	+

In the above discussions, we focus on the case that the valley is located at K or $-K$ point. Now we generalize the valley polarization rules to generic \mathbf{k} points. Under the symmetries of G_3 in 2D hexagonal lattices, the energy level and Berry curvature remain unchanged. The valleys protected by above symmetries are defined as equivalent valleys. Then the rule for generating valley polarization can be generalized to that all the enforced symmetries connecting nonequivalent valleys or reversing the sign of Berry curvature must be broken. And the rule for manipulating valley polarization remains unchanged. Based on these generalized rules, we can derive the same five valley-polarized groups ($P3, P312', P3m'1, P\bar{6}, P\bar{6}m'2'$) for the high symmetry line ΓK or KM as that of K point. Hence, the results of transforming G_{nv} to G_v and switching valley DOF for K point can be directly applied to the case of ΓK or KM . Besides, the valley polarization can be generated in groups $P3, P32'1, P31m', P\bar{6}, P\bar{6}2'm'$ along the high symmetry line ΓM , and be generated in group $P3$ for other generic \mathbf{k} points. The valley DOF in these cases can also be switched by reversing the magnetization, reversing an external field or interlayer sliding (Sec. 4 of the Supplemental Material [30]).

III. VALLEY POLARIZATION IN FeCl₂, TcGeSe₃ AND CrOBr

The above valley polarization rules are applicable to the well-known valleytronic systems with space group (SG) $P\bar{6}m2$ and provide a unified framework for understanding the generation and manipulation of valley polarization (Sec. 5 of the Supplemental Material [30]). We then apply the valley polarization rules to magnetic systems with SG $P\bar{3}m1$ and $P\bar{3}1m$, and verify the rules using density functional theory (DFT) calculations. Monolayer FeCl₂ with SG $P\bar{3}m1$ has been experimentally synthesized [34,35]. It has out-of-plane magnetic moment [36,37] and thus has the DSSG $P\bar{3}m'1 = G_v \otimes \{1, \bar{1}\}$, where $G_v = P\bar{3}m'1$, as shown in the upper panel of Fig. 2(a). According to the rules shown in Fig. 1, it does not have valley polarization, but valley polarization can be induced by applying an electric field and reversed by switching magnetic moment. As shown in the middle panel of Fig. 2(a) and Fig. S2 [30], the valleys in K and $K' = -K$ are energetically degenerate due to symmetry $\bar{1}G_v$. Besides, $\bar{1}G_v$ also gives rise to opposite layer polarizations at K and $-K$ valleys. Under an out-of-plane electric field [Fig. 2(b)], the symmetry $\bar{1}G_v$ is broken. Therefore, the non-valley-polarized group $P\bar{3}m'1$ transforms into valley-polarized group $G_v = P\bar{3}m'1$, enabling the generation of valley polarization. Since $-K$ valley has a positive layer polarization, its energy level moves downward compared to that of K valley under the downward electric field [28,33], leading to a valley splitting with energy difference of 12 meV [the middle panel of Fig. 2(b)]. The Berry curvature distribution remains nearly unchanged [the lower panels of Figs. 2(a) and 2(b)]. Having achieved the valley polarization, we then consider how to switch it. The valley DOF cannot be switched by flipping the direction of electric field as the connection operation $N_s = \bar{1}$ preserves the sign of Berry curvature. Hence, we must flip the direction of magnetic moment [Fig. 2(c)], since $N_s = 1'$ guarantees the reversal of Berry curvature [the lower panel of Fig. 2(c)].

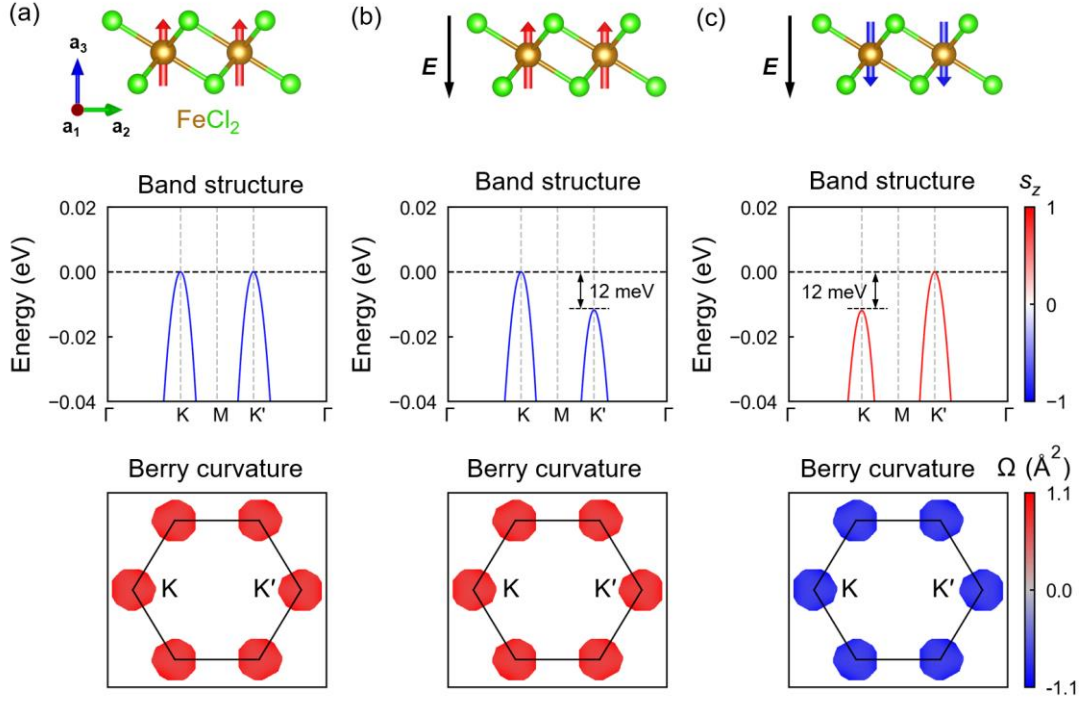


FIG. 2. The configurations, band structures and Berry curvatures of monolayer FeCl_2 (a) with an upward magnetic moment and without external electric field, (b) with an upward and (c) downward magnetic moment under an external electric field (E) of -0.05 V/\AA . In all upper panels, the red (blue) arrow denotes the upward (downward) magnetic moment. The black arrow denotes the electric field. In all middle panels, K' denotes $-K$, and the Fermi level is set to zero. The red (blue) lines denote the bands contributed by upward (downward) spin. Lower panels show the Berry curvature distributions around K and $-K$ valleys for the valence band. The red (blue) color denotes the positive (negative) Berry curvature.

Monolayer TcGeSe_3 with SG $P\bar{3}1m$ also has out-of-plane magnetic moment [38], described by the non-valley-polarized group $P\bar{3}1m'$. According to the rules in Fig. 1, valley polarization is prohibited and cannot be induced by an electric field, in contrast to monolayer FeCl_2 . But valley polarization can be generated by a combination of bilayer stacking and an external electric field, and can be further reversed via flipping the electric field when the bilayer has an interlayer AFM ordering. We stack TcGeSe_3 bilayers with the stacking operator $\hat{O} = \{m_{001}|\mathbf{t}\}$ and perform DFT calculations to

identify the magnetic ground state and valley polarization. The bilayer with $\mathbf{t} = (\frac{1}{3}, \frac{2}{3})$ has interlayer AFM ground state [Fig. 3(a)] and thus has the DSSG $P321 = G_v \cup 2_{100}G_v$, where $G_v = P3$. The conduction band is doubly degenerated at K point [the middle panel of Fig. 3(a) and Fig. S3 [30]], with zero net Berry curvature enforced by symmetries $2_{100}G_v$ [the lower panel of Fig. 3(a)]. Applying an out-of-plane electric field breaks the symmetry $2_{100}G_v$ and transforms the DSSG $P321$ into the valley-polarized group $P3$ [Fig. 3(b)]. The electric field lifts the band degeneracy and induces a valley polarization [the middle and lower panels of Fig. 3(b)]. By flipping the electric field, valley DOF is switched since $N_s = 2_{100}$ reverses the sign of Berry curvature [the middle and lower panels of Fig. 3(c)]. Meanwhile, the spin and layer DOFs are also switched, indicating that the switchable anomalous Hall effect is locked with valley, spin and layer DOFs [39,40]. However, valley DOF cannot be switched by shifting top layer with respect to bottom layer with $\mathbf{t} = (\frac{1}{3}, -\frac{1}{3})$ as $N_s = m'_{120}$ preserves the sign of the out-of-plane magnetization and thus the sign of Berry curvature under the electric field. Besides, for another stacking TcGeSe₃ bilayer with $\hat{O} = \{1 | (\frac{1}{3}, \frac{2}{3})\}$, it has the interlayer AFM ground state with non-valley-polarized group $P\bar{3}'$. Its conduction band is doubly degenerated at all \mathbf{k} points and has zero net Berry curvature and thus vanishing valley polarization due to the symmetry $\bar{1}'$. Valley polarization can also be induced by applying an out-of-plane electric field and reversed by flipping the field (see details in Sec. 6 of the Supplemental Material [30]).

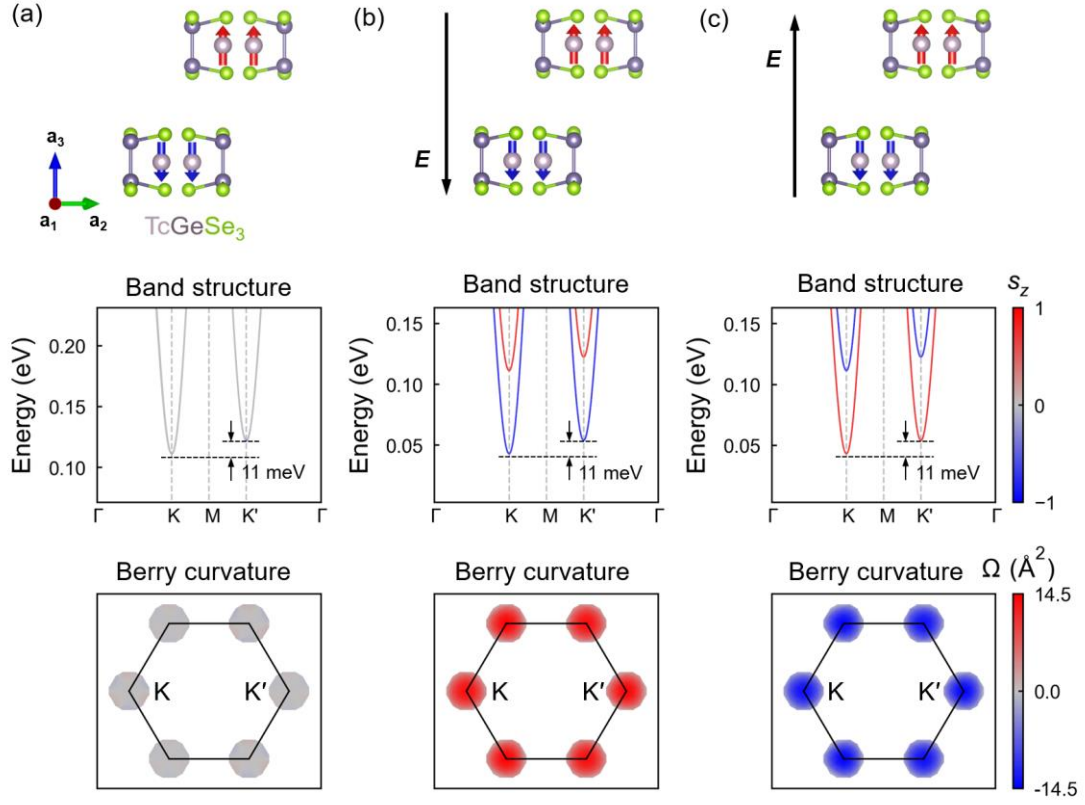


FIG. 3. The configurations, band structures and Berry curvatures of AFM bilayer TcGeSe_3 stacked by operator $\hat{O} = \left\{ m_{001} \left[\frac{1}{3}, \frac{2}{3} \right] \right\}$ (a) without an external electric field, (b) with a downward ($E = -0.01 \text{ V/\AA}$) and (c) upward external electric field ($E = 0.01 \text{ V/\AA}$). In all upper panels, the red (blue) arrow denotes the upward (downward) magnetic moment. The black arrow denotes the electric field. In all middle panels, K' denotes $-K$, and the Fermi level is set to zero. The red (blue) lines denote the bands contributed by upward (downward) spin. The grey color denotes zero spin polarization. Lower panels show the Berry curvature distributions around K and $-K$ valleys for the conduction band. The red, grey and blue colors denote the positive, zero and negative net Berry curvature, respectively.

Besides, we apply our valley polarization rules to a case where valleys are located at generic \mathbf{k} points. Monolayer CrOBr with SG $P3m1$ has out-of-plane magnetization [41], represented by the DSSG $P3m'1$. The rules in Fig. 1 predict that CrOBr has a spontaneous valley polarization when its valleys are located along ΓK line. The valley polarization can be reversed by switching the magnetic moment. DFT calculations in

Ref. [41] have identified the valley splitting in the valence band. Here, we demonstrate the generation of valley polarization by a further characterization of Berry curvatures. When the magnetic moment of CrOBr is upward [Fig. 4(a)], the VBM locates at three equivalent valleys V_2 with nonzero Berry curvatures [the middle and lower panels of Fig. 4(a) and Fig. S5 [30]], indicating the emergence of valley polarization. When reversing its magnetic moment, the valley DOF is switched due to $N_s = 1'$ [the middle and lower panels of Fig. 4(b)].

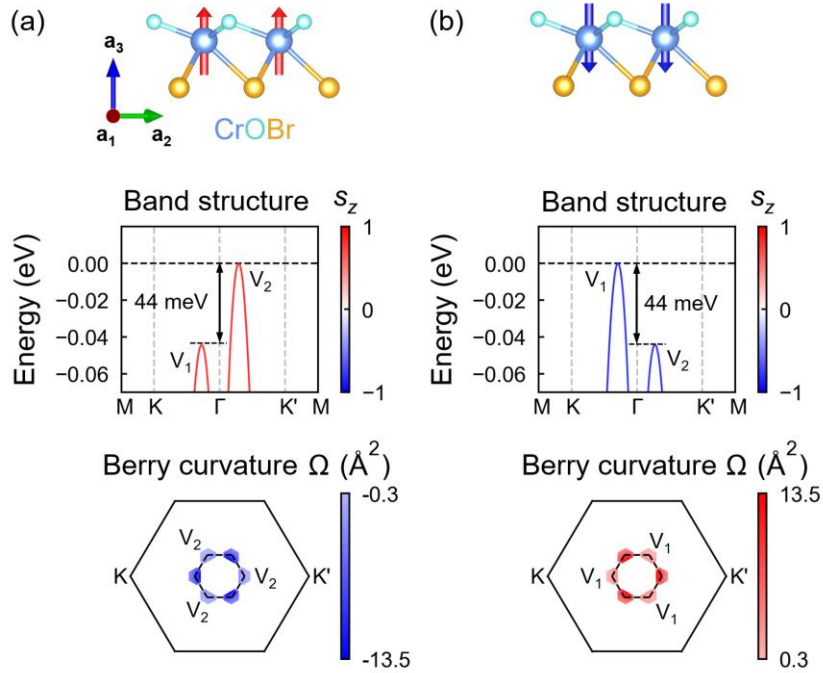


FIG. 4. The configurations, band structures and Berry curvatures of monolayer CrOBr (a) with an upward magnetic moment and (b) downward magnetic moment. In upper panels, the red (blue) arrow denotes the upward (downward) magnetic moment. In middle panels, K' denotes $-K$. V_1 and V_2 denote the valley located at ΓK and $\Gamma K'$ line, respectively. The Fermi level is set to zero. The red (blue) lines denote the bands contributed by upward (downward) spins. Lower panels show the Berry curvature distributions around K and $-K$ valleys for the valence band. The red (blue) color denotes the positive (negative) Berry curvature.

IV. SUMMARY AND DISCUSSION

In conclusion, we provide general rules for generating valley polarization and

switching valley DOF. Based on symmetry analysis, we identify all DSSGs permitting valley polarization and reveal that the connection operation determines the switching of valley DOF. Moreover, the valley polarization rules are also applicable to other 2D and 3D lattices, regardless of the valley DOF is associated with either the Berry curvature or the optical selection rule (Sec. 7 of the Supplemental Material [30]). Our findings provide a unified framework for predicting valley-polarized systems and offer insights for other relevant fields such as magnetoelectrics and multiferroics.

ACKNOWLEDGMENT

The authors thank Boxuan Li for helpful discussions. This work is supported by funds from the National Natural Science Foundation of China (62488201, 52272172, 11974045), the Major Program of the National Natural Science Foundation of China (92163206), the National Key Research and Development Program of China (2022YFA1204100, 2021YFA1201501).

*Corresponding authors: jtsun@bit.edu.cn, sxdu@iphy.ac.cn

- [1] J. R. Schaibley, H. Y. Yu, G. Clark, P. Rivera, J. S. Ross, K. L. Seyler, W. Yao, and X. D. Xu, Valleytronics in 2D materials, *Nat. Rev. Mater.* **1**, 16055 (2016).
- [2] X.-W. Shen, H. Hu, and C.-G. Duan, in *Spintronic 2D Materials* (Elsevier, 2020), pp. 65.
- [3] D. Xiao, W. Yao, and Q. Niu, Valley-contrasting physics in graphene: magnetic moment and topological transport, *Phys. Rev. Lett.* **99**, 236809 (2007).
- [4] A. Rycerz, J. Tworzydło, and C. W. J. Beenakker, Valley filter and valley valve in graphene, *Nat. Phys.* **3**, 172 (2007).
- [5] R. V. Gorbachev *et al.*, Detecting topological currents in graphene superlattices, *Science* **346**, 448 (2014).
- [6] M. Sui *et al.*, Gate-tunable topological valley transport in bilayer graphene, *Nat. Phys.* **11**, 1027 (2015).
- [7] A. R. Akhmerov and C. W. Beenakker, Detection of valley polarization in graphene by a superconducting contact, *Phys. Rev. Lett.* **98**, 157003 (2007).
- [8] W. Yao, D. Xiao, and Q. Niu, Valley-dependent optoelectronics from inversion symmetry breaking, *Phys. Rev. B* **77**, 235406 (2008).
- [9] D. Xiao, G. B. Liu, W. Feng, X. Xu, and W. Yao, Coupled spin and valley physics in monolayers of MoS₂ and other group-VI dichalcogenides, *Phys. Rev. Lett.* **108**, 196802 (2012).
- [10] X. Xu, W. Yao, D. Xiao, and T. F. Heinz, Spin and pseudospins in layered transition

- metal dichalcogenides, *Nat. Phys.* **10**, 343 (2014).
- [11] G. Aivazian *et al.*, Magnetic control of valley pseudospin in monolayer WSe₂, *Nat. Phys.* **11**, 148 (2015).
- [12] D. MacNeill, C. Heikes, K. F. Mak, Z. Anderson, A. Kormányos, V. Zolyomi, J. Park, and D. C. Ralph, Breaking of valley degeneracy by magnetic field in monolayer MoSe₂, *Phys. Rev. Lett.* **114**, 037401 (2015).
- [13] Y. C. Cheng, Q. Y. Zhang, and U. Schwingenschlögl, Valley polarization in magnetically doped single-layer transition-metal dichalcogenides, *Phys. Rev. B* **89**, 155429 (2014).
- [14] J. Qi, X. Li, Q. Niu, and J. Feng, Giant and tunable valley degeneracy splitting in MoTe₂, *Phys. Rev. B* **92**, 121403 (2015).
- [15] Q. Zhang, S. A. Yang, W. Mi, Y. Cheng, and U. Schwingenschlögl, Large Spin - Valley Polarization in Monolayer MoTe₂ on Top of EuO(111), *Adv. Mater.* **28**, 959 (2015).
- [16] E. J. Sie, J. W. McIver, Y.-H. Lee, L. Fu, J. Kong, and N. Gedik, Valley-selective optical Stark effect in monolayer WS₂, *Nat. Mater.* **14**, 290 (2014).
- [17] J. Kim, X. Hong, C. Jin, S.-F. Shi, C.-Y. S. Chang, M.-H. Chiu, L.-J. Li, and F. Wang, Ultrafast generation of pseudo-magnetic field for valley excitons in WSe₂ monolayers, *Science* **346**, 1205 (2014).
- [18] L. Du, T. Hasan, A. Castellanos-Gomez, G.-B. Liu, Y. Yao, C. N. Lau, and Z. Sun, Engineering symmetry breaking in 2D layered materials, *Nat. Rev. Phys.* **3**, 193 (2021).
- [19] Z. Gong, G. B. Liu, H. Yu, D. Xiao, X. Cui, X. Xu, and W. Yao, Magnetoelectric effects and valley-controlled spin quantum gates in transition metal dichalcogenide bilayers, *Nat. Commun.* **4**, 2053 (2013).
- [20] W. Y. Tong, S. J. Gong, X. Wan, and C. G. Duan, Concepts of ferrovalley material and anomalous valley Hall effect, *Nat. Commun.* **7**, 13612 (2016).
- [21] P. Zhao, Y. Ma, C. Lei, H. Wang, B. Huang, and Y. Dai, Single-layer LaBr₂: Two-dimensional valleytronic semiconductor with spontaneous spin and valley polarizations, *Appl. Phys. Lett.* **115**, 261605 (2019).
- [22] C. Luo, X. Peng, J. Qu, and J. Zhong, Valley degree of freedom in ferromagnetic Janus monolayer H-VSSe and the asymmetry-based tuning of the valleytronic properties, *Phys. Rev. B* **101**, 245416 (2020).
- [23] P. Jiang, L. Kang, Y.-L. Li, X. Zheng, Z. Zeng, and S. Sanvito, Prediction of the two-dimensional Janus ferrovalley material LaBrI, *Phys. Rev. B* **104**, 035430 (2021).
- [24] T. Zhang, X. Xu, B. Huang, Y. Dai, and Y. Ma, 2D spontaneous valley polarization from inversion symmetric single-layer lattices, *npj Comput. Mater.* **8**, 64 (2022).
- [25] K. F. Mak, K. He, J. Shan, and T. F. Heinz, Control of valley polarization in monolayer MoS₂ by optical helicity, *Nat. Nanotechnol.* **7**, 494 (2012).
- [26] T. Cao *et al.*, Valley-selective circular dichroism of monolayer molybdenum disulphide, *Nat. Commun.* **3**, 887 (2012).
- [27] K. F. Mak, K. L. McGill, J. Park, and P. L. McEuen, The valley Hall effect in MoS₂ transistors, *Science* **344**, 1489 (2014).
- [28] W.-Y. Tong and C.-G. Duan, Electrical control of the anomalous valley Hall effect in antiferrovalley bilayers, *npj Quantum Mater.* **2**, 47 (2017).

- [29]X. Liu, A. P. Pyatakov, and W. Ren, Magnetoelectric coupling in multiferroic bilayer VS₂, *Phys. Rev. Lett.* **125**, 247601 (2020).
- [30]See Supplemental Material for details about group theory analysis, valley polarization in known systems, computational methods, DFT results of valley polarization in FeCl₂, TcGeSe₃ and CrOBr, and valley polarization in other 2D and 3D lattices, which includes Refs. [12,20,24,29,31-33,38-64].
- [31]J. Ji, G. Yu, C. Xu, and H. J. Xiang, General theory for bilayer stacking ferroelectricity, *Phys. Rev. Lett.* **130**, 146801 (2023).
- [32]L. Elcoro *et al.*, Double crystallographic groups and their representations on the Bilbao Crystallographic Server, *J. Appl. Crystallogr.* **50**, 1457 (2017).
- [33]Z. M. Yu, S. Guan, X. L. Sheng, W. Gao, and S. A. Yang, Valley-layer coupling: a new design principle for valleytronics, *Phys. Rev. Lett.* **124**, 037701 (2020).
- [34]X. Zhou *et al.*, Atomically thin 1T-FeCl₂ grown by molecular-beam epitaxy, *J. Phys. Chem. C* **124**, 9416 (2020).
- [35]S. Jiang *et al.*, General synthesis of 2D magnetic transition metal dihalides via trihalide reduction, *ACS Nano* **17**, 363 (2022).
- [36]A. S. Botana and M. R. Norman, Electronic structure and magnetism of transition metal dihalides: Bulk to monolayer, *Phys. Rev. Mater.* **3**, 044001 (2019).
- [37]Q. Yao, J. Li, and Q. Liu, Fragile symmetry-protected half metallicity in two-dimensional van der Waals magnets: A case study of monolayer FeCl₂, *Phys. Rev. B* **104**, 035108 (2021).
- [38]J.-Y. You, Z. Zhang, X.-J. Dong, B. Gu, and G. Su, Two-dimensional magnetic semiconductors with room Curie temperatures, *Phys. Rev. Res.* **2**, 013002 (2020).
- [39]A. Gao *et al.*, Layer Hall effect in a 2D topological axion antiferromagnet, *Nature* **595**, 521 (2021).
- [40]T. Zhang, X. Xu, B. Huang, Y. Dai, L. Kou, and Y. Ma, Layer-polarized anomalous Hall effects in valleytronic van der Waals bilayers, *Mater. Horiz.* **10**, 483 (2023).
- [41]R. J. Sun, R. Liu, J. J. Lu, X. W. Zhao, G. C. Hu, X. B. Yuan, and J. F. Ren, Reversible switching of anomalous valley Hall effect in ferrovalley Janus 1T-CrOX (X=F,Cl,Br,I) and the multiferroic heterostructure CrOX/In₂Se₃, *Phys. Rev. B* **105**, 235416 (2022).
- [42]Z. Zhang, W. Wu, G.-B. Liu, Z.-M. Yu, S. A. Yang, and Y. Yao, Encyclopedia of emergent particles in 528 magnetic layer groups and 394 magnetic rod groups, *Phys. Rev. B* **107**, 075405 (2023).
- [43]K. Shinohara, A. Togo, and I. Tanaka, Algorithms for magnetic symmetry operation search and identification of magnetic space group from magnetic crystal structure, *Acta Crystallogr A Found Adv* **79**, 390 (2023).
- [44]G.-B. Liu, Z. Zhang, Z.-M. Yu, and Y. Yao, MSGCorep: A package for corepresentations of magnetic space groups, *Comput. Phys. Commun.* **288**, 108722 (2023).
- [45]J. Deng, J. B. Pan, Y. F. Zhang, and S. X. Du, Database construction of two-dimensional charged building blocks for functional-oriented material design, *Nano Lett.* **23**, 4634 (2023).
- [46]V. Wang, N. Xu, J.-C. Liu, G. Tang, and W.-T. Geng, VASPKIT: A user-friendly

interface facilitating high-throughput computing and analysis using VASP code, *Comput. Phys. Commun.* **267**, 108033 (2021).

[47] L. Elcoro, B. J. Wieder, Z. Song, Y. Xu, B. Bradlyn, and B. A. Bernevig, Magnetic topological quantum chemistry, *Nat. Commun.* **12**, 5965 (2021).

[48] X.-W. Shen, W.-Y. Tong, S.-J. Gong, and C.-G. Duan, Electrically tunable polarizer based on 2D orthorhombic ferrovalley materials, *2D Mater.* **5**, 011001 (2017).

[49] M. Wu and X. C. Zeng, Intrinsic ferroelasticity and/or multiferroicity in two-dimensional phosphorene and phosphorene analogues, *Nano Lett.* **16**, 3236 (2016).

[50] H.-J. Kim, C. Li, J. Feng, J.-H. Cho, and Z. Zhang, Competing magnetic orderings and tunable topological states in two-dimensional hexagonal organometallic lattices, *Phys. Rev. B* **93**, 041404 (2016).

[51] S. P. Ong *et al.*, Python Materials Genomics (pymatgen): A robust, open-source python library for materials analysis, *Comput. Mater. Sci.* **68**, 314 (2013).

[52] K. Momma and F. Izumi, VESTA 3 for three-dimensional visualization of crystal, volumetric and morphology data, *J. Appl. Crystallogr.* **44**, 1272 (2011).

[53] D. Xiao, M.-C. Chang, and Q. Niu, Berry phase effects on electronic properties, *Rev. Mod. Phys.* **82**, 1959 (2010).

[54] N. Nagaosa, J. Sinova, S. Onoda, A. H. MacDonald, and N. P. Ong, Anomalous Hall effect, *Rev. Mod. Phys.* **82**, 1539 (2010).

[55] S. Grimme, J. Antony, S. Ehrlich, and H. Krieg, A consistent and accurate ab initio parametrization of density functional dispersion correction (DFT-D) for the 94 elements H-Pu, *J. Chem. Phys.* **132**, 154104 (2010).

[56] C. Bradley and A. Cracknell, *The mathematical theory of symmetry in solids: representation theory for point groups and space groups* (Oxford University Press, 2010).

[57] J. D. Hunter, (IEEE Computer Society, 2007), pp. 90.

[58] M. I. Aroyo, J. M. Perez-Mato, C. Capillas, E. Kroumova, S. Ivantchev, G. Madariaga, A. Kirov, and H. Wondratschek, Bilbao Crystallographic Server: I. Databases and crystallographic computing programs, *Z. Kristallogr. - Cryst. Mater.* **221**, 15 (2006).

[59] M. I. Aroyo, A. Kirov, C. Capillas, J. M. Perez-Mato, and H. Wondratschek, Bilbao Crystallographic Server. II. Representations of crystallographic point groups and space groups, *Acta Crystallogr A* **62**, 115 (2006).

[60] G. Kresse and D. Joubert, From ultrasoft pseudopotentials to the projector augmented-wave method, *Phys. Rev. B* **59**, 1758 (1999).

[61] S. L. Dudarev, G. A. Botton, S. Y. Savrasov, C. J. Humphreys, and A. P. Sutton, Electron-energy-loss spectra and the structural stability of nickel oxide: An LSDA+U study, *Phys. Rev. B* **57**, 1505 (1998).

[62] J. P. Perdew, K. Burke, and M. Ernzerhof, Generalized gradient approximation made simple, *Phys. Rev. Lett.* **77**, 3865 (1996).

[63] G. Kresse and J. Furthmüller, Efficiency of ab-initio total energy calculations for metals and semiconductors using a plane-wave basis set, *Comput. Mater. Sci.* **6**, 15 (1996).

[64] J. F. Cornwell, *Group theory in physics* (Academic Press, 1984), Volume I .